Symmetrical Spread of the Sun's Position at the Equator:
A Potential for Optimum with Diverse Access

Budi Rudianto* iD .

Department of Architecture, Faculty of Engineering, Universitas Tridinanti,
Jl. Kapten Marzuki No. 2446, Palembang 30129, Indonesia.

E-*mail:* brudianto765@gmail.com .

ARTICLE INFO.

ABSTRACT

Buildings that use renewable energy sources, such as sunlight with solar collector technology, are in demand to face climate change. The position of the sun is a pivotal reference for determining the optimum of solar collectors. There are two differences in the optimum results in the equatorial region due to the different perceptions in defining the sun's position. This study highlights the optimum orientation that is not perpendicular because it reflects the actual position that spreads at the equator. This study aims to prove the sun's position that spreads in the equatorial region and to show the optimum potential with varied accesses.

The investigation is conducted through the angular coordinates of altitude and azimuth. The methodology used is simulation calculation and descriptive analysis by comparison. The simulation calculation uses SunEarthTools.com, based on equations from astronomical algorithms by Michalsky. The validation uses the NOAA Solar Position Calculator, based on equations from astronomical algorithms by Meeus. The targets of the study are to make a profile of the performance of the sun's position and a profile of the opportunity for the sloped surfaces to accept access. The sun-earth relationship and the season period are the factors that cause differences in the angular range of the sun's position for each latitude zone. The results prove that the equatorial region has a more spacious range of orientation and a relatively balanced high of elevation in the four main cardinal directions than other regions. The highest points occur twice during the equinoxes for the balanced position between the east and west orientations, and the farthest points happen in the summer solstices for the balanced position between the north and south orientations.

The spreading position allows two low-inclined surfaces facing opposite orientations to be exposed simultaneously for long periods, especially in the equinoxes. This study contributes a theoretical insight into the optimum at the equator that has potency for optimum with diverse access.

<h1 dir="rtl">التوزيع المتناظر لموقع الشمس عند خط الاستواء: إمكانية لتحقيق الأمثل مع الوصول المتنوع</h1>

<p dir="rtl">بودي روديانتو.</p>

<p dir="rtl">ملخـص: المباني التي تستخدم مصادر الطاقة المتجددة، مثل ضوء الشمس مع تكنولوجيا المجمعات الشمسية، مطلوبة لمواجهة تغير المناخ. موقع الشمس هو مرجع محوري لتحديد الأمثل لجمعيات الطاقة الشمسية. هناك اختلافان في النتائج المثلى في المنطقة الاستوائية بسبب الاختلافات في تحديد موقع الشمس. تسلط هذه الدراسة الضوء على الاتجاه الأمثل الذي ليس عمودياً لأنه يعكس الوضع الفعلي الذي ينتشر عند خط الاستواء. تهدف هذه الدراسة إلى إثبات موقع الشمس الذي ينتشر في المنطقة الاستوائية وإظهار الإمكانات المثلى مع الوصول المتنوع. تُجرى التحقيقات من خلال الإحداثيات الزاوية للارتفاع والزاوية الأفقية. المنهجية المستخدمة هي حساب المحاكاة والتحليل الوصفي بالمقارنة. يستخدم حساب المحاكاة موقع SunEarthTools.com، استنادًا إلى معادلات من الخوارزميات الفلكية لمايكلسكي. تستخدم عملية التحقق حاسبة NOAA لموقع الشمس، المستندة إلى معادلات من الخوارزميات الفلكية لـ Meeus. أهداف الدراسة هي إنشاء ملف عن أداء موقع الشمس وملف عن فرصة الأسطح المائلة لقبول الوصول. علاقة الشمس بالأرض وفترة الموسم هما العاملان اللذان يسببان اختلافات في النطاق الزاوي لموقع الشمس لكل منطقة عرضية. تثبت النتائج أن المنطقة الاستوائية تتمتع بنطاق أوسع من التوجه وارتفاع متوازن نسبياً في الاتجاهات الأربعة الرئيسية أكثر من المناطق الأخرى. تحدث أعلى النقاط مرتين خلال الاعتدالات من أجل الوضع المتوازن بين الاتجاهات الشرقية والغربية، وتحدث النقاط الأبعد في الانقلابات الصيفية من أجل الوضع المتوازن بين الاتجاهات الشمالية والجنوبية. تسمح الوضعية المنتشرة بتعرض سطحين مائلين قليلاً يواجهان اتجاهات متقابلة في نفس الوقت لفترات طويلة، خاصة في الاعتدالات. تساهم هذه الدراسة برؤية نظرية حول الأمثل عند خط الاستواء الذي يتمتع بإمكانية الوصول المتنوع للأمثل .</p>

<p dir="rtl">الكلمات المفتاحية – الإحداثي الزاوي، خط العرض، الاتجاهات المتقابلة، حساب المحاكاة، زاوية الميل الشمسي.</p>

1. INTRODUCTION

Excessive use of non-renewable energy in the building sector contributes to climate change [1]. Sustainable development means meeting current needs while also taking into account future availability. Goal 13 of the 17 SDGs (Sustainable Development Goals) is to take urgent action to combat climate change and its impacts. One strategy to address climate change is to use renewable energy sources, such as wind and sunlight [2]. Sunlight is the most abundant renewable energy resource available in nature. Solar collector technology converts sunlight into electrical and thermal energies [3].

Solar collector systems are a prominent renewable energy source that contributes to decreasing emissions [4]. The tilt angle and orientation are the parameters to face the surfaces capturing solar radiation. The rule of thumb for maximum solar radiation is the tilt angle close to the latitude with the orientation towards the equator. Duffie et al. [5] proposed an equation for optimum that refers to latitude, which is $\beta_{opt} = (\varphi + 15°) \pm 15°$, where φ represents the latitude and (+) for summer and (-) for winter. Studies in the subtropical regions focused on the optimum of the tilt angle. The orientation was sure due to the concentrated sun's position at the equator. In the north latitude, Kim et al. [6] in Daegu, Korea (Lat. 35.87°N) and Sevik et al. [7] in Corum, Turkey (Lat. 40.55°N) showed the optimum orientation facing south. In the south, Cabral et al. [8] in Florianopolis (Lat. 27.59°S) and Porto Alegre, Brazil (Lat. 30.03°S) showed the optimum orientation facing north. Studies of optimum in high-latitude zones show a match between the sun's position and the optimum orientation.

There are two differences in the optimum results related to orientation in the equatorial region. Most previous studies use the principle of the subtropical areas. Matius et al. [9] in Sabah (Lat. 6.25°N) and Njoku et al. [10] in Nigeria (Lat. 4°-14°N) showed the annual optimum orientation facing south. Afandi et al. [11] in Jakarta (Lat. 6.30°S) and Sugirianta [12] in Bali, Indonesia (Lat. 8.81°S) showed the yearly optimum orientation facing north. On the other hand, several studies notice the character of the position that spreads in the equatorial region. Serrano-Guerrero et al. [13] in Ecuador (Lat. 2.88°S), Khoo et al. [14] in Singapore (Lat. 1.37°N), Bari [15] in Malaysia (Lat. 1°N-7°N), Lau et al. [16] in Southeast Asia area, Cronemberger et al. [17] in Brazil, Tsoukpoe [18] in Africa area (Lat. 0°-15°N), and Mukisa & Zamora [19] in Uganda (Lat. 1.3°S-7°N) showed the annual optimum orientation facing not perpendicular. This study focuses on the second group with the optimum orientation facing diagonal, which describes the actual character of the sun's position at the equator. This study wants to provide a firm understanding that the equator has a geographical advantage in the sun's position. Hence, the target stages of the study are to make a profile of the performance of the sun's position and a profile of the opportunity for the sloped surfaces to receive access.

Most previous studies of the sun's position discussed the models or methods of calculation. The field of astronomy is the most competent to discuss it [30], [32], [33], [34]. Meanwhile, the field of solar energy discusses the effect of the position getting the optimum condition of the solar collectors [35]. This study uses the optimum studies from the field of solar energy for design purposes. In the past, buildings in the equatorial region have high-sloped pitched roofs to reduce heat gain from the intensity of sunlight. In technological developments, the roof function is utilized to obtain energy, forcing the roof with a low tilt angle to get maximum exposure to sunlight. There is a paradigm shift in roof designs in the equatorial region from avoiding to capturing sunlight. So far, no architectural studies have been seen to significantly exploit the spreading sun's position for design purposes.

Most studies here use the high latitude approach, so the implications are with uniform configuration. This study is on the relationship between the position of the sun and the optimum theory in the equatorial region, where there is a disregard for the actual position. Thus, the novelty of this research is to make a profile of the performance of the sun's position to prove the position that spreads on many orientations in the equatorial region and create a profile of the opportunity for the sloped surfaces facing many directions to show the optimum potential with diverse access.

According to UN [20], more than half of the people in the world reside in cities. Thus, urban settlement areas have dominated the city face. According to UN [21], the use of clean energy at the community level is vital in mitigating the impact of climate change, as outlined in the SDGs: SDGs-7 (affordable and clean energy) and SDGs-11 (sustainable cities and communities). The varied roof configurations with BIPV applications in urban settlements along the equator have tremendous potential as solar energy producers. Therefore, this study aims to demonstrate in quantity the spreading sun's position in the equatorial region, which allows optimum with varying accesses.

2. LITERATURE AND METHODOLOGY

2.1. Solar Geometry

Figure 1 illustrates the movement of the Earth around the sun. The Earth rotates on an oblique axis and revolves around the sun in a fully elliptical orbit in a year (365 days). The average sun-earth distance occurs on April 4 and October 5 at 1.496 x 1011 m, known as 1 AU (Astronomical

Unit). The farthest distance is aphelion, on July 4 at 1.017 AU. The shortest distance is perihelion, on January 3 at 0.983 AU [22]. The elliptical orbit causes the varying distance between the Earth and the sun to follow the time function.

Figure 2 shows the variations of declination angle in four seasonal periods. The declination angle (δ) is the angle between the direction of the sunray and the equator plane. The declination angle has an interval of $+23.45° \leq \delta \leq -23.45°$. $\delta = +23.45°$ is the summer solstice in the north, 20-21 June in the Tropic of Cancer at latitude 23.45°N. $\delta = -23.45°$ is the summer solstice in the south, 21-22 December in the Tropic of Capricorn at latitude 23.45°S. $\delta = 0°$ is the equinoxes at the equator, which occur twice on 20-21 March (vernal) and 22-23 September (autumnal) [23]). The inclination of the axis causes the varying intensity of sunray at a region, shown by the bright dark of the Earth's surface due to the declination shift to follow the time function. A bright surface in the north or south indicates its location directly facing the sun during the summer. The brightest surface at the equator indicates its location perpendicularly facing the sun during the equinoxes.
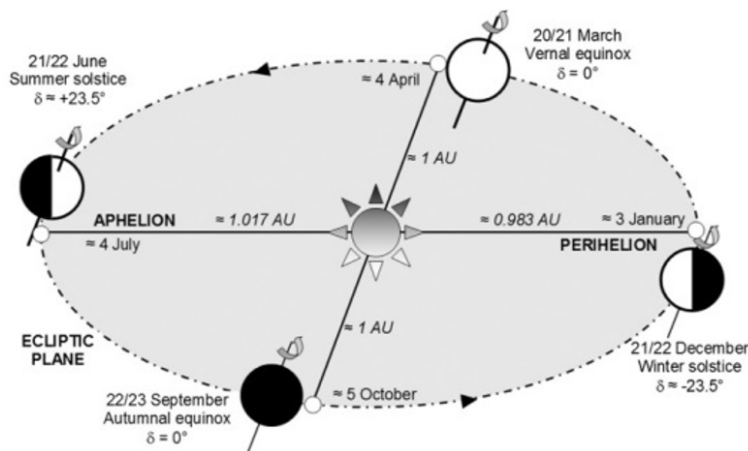
Figure 1. The motion of the Earth around the sun [22].
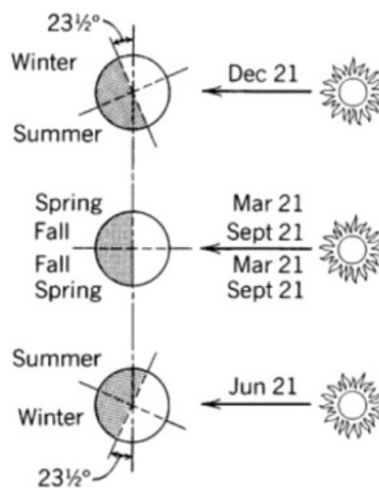
Figure 2. The variations of declination angle [23].

To know the sun's position by plotting the angular coordinates onto the horizontal plane for azimuth angle and onto the vertical plane for altitude angle. The horizontal sun-path diagram is a circular plane consisting of seven lanes. The northernmost and southernmost lanes each are on June 21 ($\delta = +23.45°$) and December 21 ($\delta = -23.45°$), respectively. The center lanes overlap twice in March 21 and September 21 ($\delta = 0°$) in opposite directions. The more curved line in June

indicates the closest to the observer in the north. The vertical sun-path diagram is a semicircular plane. The tallest line in June indicates the closest to the observer in the north [5], [24].

2.2. Sun-path Diagram

Figure 3 displays the horizontal sun-path diagram at three latitude locations: 1°N, 48°N, and 27°S. The three-horizontal sun-path diagrams represent the world zones, namely Singapore (Lat. 1°N), Freiburg, Germany (Lat. 48°N), and Florianopolis, Brazil (Lat. 27°S). Singapore at the equator shows a balanced curved line in the opposite directions between the summer solstice in the north and the summer solstice in the south. Freiburg in the north has a more curved line on the summer solstice (June 21) than the solstice in the south. On the other hand, Florianopolis in the south has a more curved line on the summer solstice (December 21) than the solstice in the north [25].
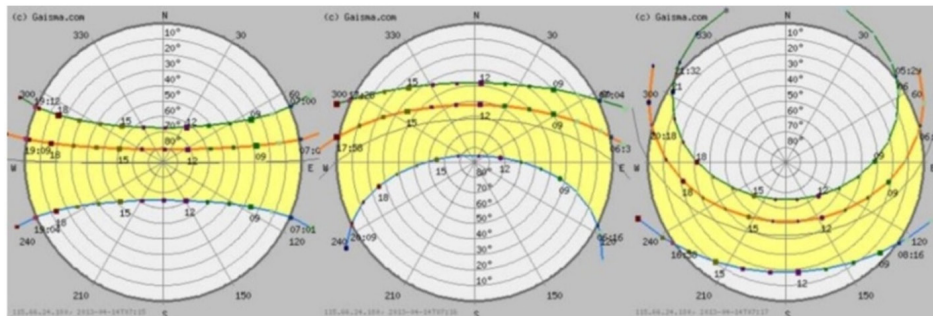
Figure 3. The horizontal sun-path diagram at three latitudes: 1°N, 48°N, and 27°S [25].

Figure 4a shows the vertical sun path during the summer solstices. The sun passes with the highest position during the summer solstice in the north on June 22 at latitude 23.45°N. The equinoxes and the summer solstice in the south each pass with the lower position beside. The sun passes with the highest position during the summer solstice in the south on December 21 at latitude 23.45°S. The equinoxes and the summer solstice in the north each pass with the lower position beside [26]. Figure 4b shows the vertical sun path during the equinoxes. The sun passes with the highest position during the equinoxes at the equator twice a year, each on March 21 at the vernal equinox and September 21 at the autumnal equinox. The summer solstice in the north on June 22 and the summer solstice in the south on December 22 each pass with the lower position in opposite that is flanking the equinoxes [27].
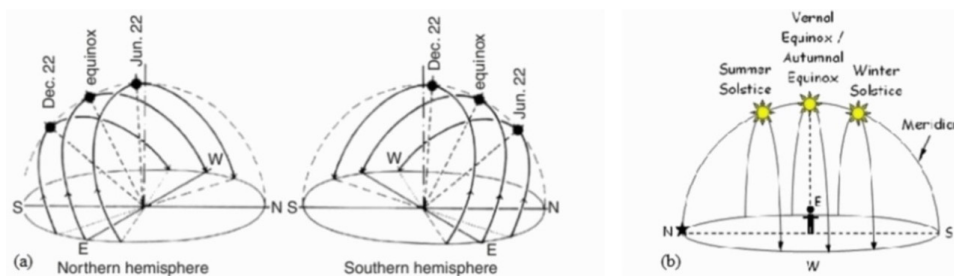
Figure 4. The vertical sun path: (a) In the summer solstices [26], (b) In the equinoxes [27].

2.3. Methodology

This study investigates the sun's position from the perspective of the field of architecture. The material analyzed is the angular coordinates from the results of simulation calculations. The methodology used is simulation calculation and analysis by comparison. Simulation

calculation helps to predict quickly the sun's position in a specific location with the output of numerical and graphical data. Descriptive analysis by comparisons connects the results between latitudes that use the same pattern of the sentence structure in a paragraph. Discussions with descriptive analysis by comparisons in paragraph format are common in architectural research. The limitation of the study is the investigation of the sun's position based on the simulation calculation with the time of observation that includes four periods of the sun's path on the same date, which describes the highest and farthest position for a year.

This study aims to prove the position that spreads in the equatorial region to show the optimum potential with many accesses. The targets to achieve it are to make a profile of the performance of the position and a profile of the opportunity for the sloped surface to gain access. There are four phases of the research as follows:

1. The first step (a) is to determine the boundaries of the latitude zone for investigation. The equatorial region lies with a range of latitude about 10° to the north and south within the tropical region span between Lat. 23.5°N and Lat. 23.5°S. The subtropical region consists of two parts in the north with a span from 23.5°N to 35°N and in the south with a range from 23.5°S to 35°S [28]. Thus, the location for investigation consists of three latitude zones. Latitude 0° represents the low-latitude zone (i.e., equatorial region), while latitudes 35°N and 35°S represent the high-latitude zones (i.e., subtropical region) in the north and south.

The first step (b) is to determine the sun's path period to observe the position for a year. There are four main periods of the path with three declination angles which represent the movement of the sun for a year, namely $\delta = +23.45°$, $\delta = -23.45°$, and $\delta = 0°$. The period on June 21 ($\delta = +23.45°$) is the northernmost position at latitude 23.45°N. December 21 ($\delta = -23.45°$) is the southernmost position at latitude 23.45°S. March 21 and September 21 ($\delta = 0°$) are the highest positions at the equator (Lat. 0°).

2. The second step is to determine how to investigate the angular coordinates in horizontal and vertical. The angular coordinates include the azimuth angle (AZI) or orientation and the altitude angle (ALT) or elevation. Figure (5a) shows three conditions of the angular coordinates for investigation. The range of the sun's position for investigation uses the average sunshine duration per day in this area. Noon is a peak of the day. The balance of the sun's position between before and after noon is an observed phenomenon. This study uses 6 hours of sunshine duration per day: 3 hours before noon and 3 hours after noon, which reflects the relative balance of the sun's position in a day.
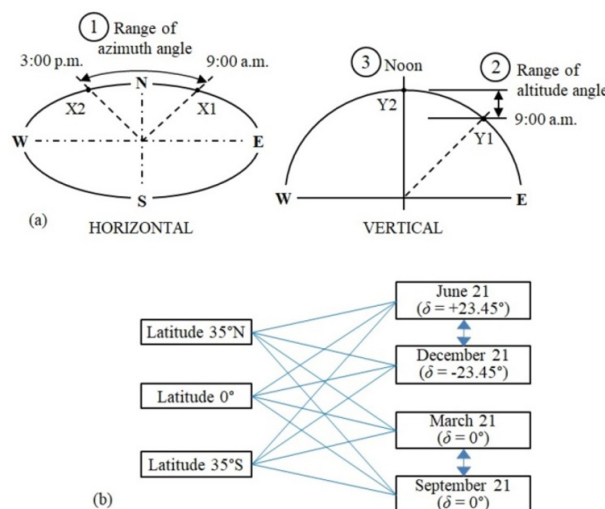
Figure 5. (a) The angular coordinates in horizontal and vertical, (b) The combinations of simulation calculations.

Three conditions of the angular coordinates in the range of hour angles for investigation are:

a). Range of azimuth angle from 9:00 a.m. to 3:00 p.m. describes the width of the movement horizontally. The horizontal range is X2 (3:00 p.m.) - X1 (9:00 a.m.).

b). Range of altitude angle from 9:00 a.m. to noon shows the high position vertically. The vertical range is Y2 (noon) - Y1 (9:00 a.m.).

c). Point of altitude angle at noon describes the highest point vertically for a day. The vertical point is Y2 (noon). All units are in degrees (°).

3. The third step (a) is to compute the sun's position, which refers to three conditions of the angular coordinates. The simulation calculation uses a free application, namely SunEarthTools. com [29]. The program calculates the position in the sky for each location on the Earth at any time of day. The calculation is based on equations from astronomical algorithms by Michalsky [30]. The program is reliable for education, work, and research. The input for the supporting data includes the angular coordinate of longitude (Lon.) 110°E, UTC +7, and the year 2021. The output is the hourly angular in the numerical and graphical data. Figure 5b shows the combinations of simulation calculations. Thus, the simulation calculations run on four main path periods, viewed from three latitudes of investigation. In total, there are twelve combinations of simulation calculations.

The third step (b) is to validate and analyze the simulation calculation results. The validation uses a free online spreadsheet calculation: the NOAA Solar Position Calculator [31]. It is a reliable tool for calculating the position at a specific time and geographical coordinates. The calculations are based on equations from astronomical algorithms by Meeus [32]. The calculations are available for a day and a year in Microsoft Excel and Open Office format. This study uses a spreadsheet calculation for a day: NOAA_Solar_Calculations_day.xls. The validation runs by juxtaposing all data from the simulation results with all data from the validation results. If the discrepancy data between the simulation results and validation is close to zero, the next steps of the research can continue.

The analysis compares the angular range in pair on the four sun path periods (i.e., June 21 and December 21, March 21 and September 21), at each latitude of investigation. Discussions refer to the theory in Figures 1 to 4. The differences found after juxtaposing the angular range in pairs among three latitudes are the characteristics of the sun's position for each latitude zone.

4. The fourth step (a) is to make a profile of the performance of the sun's position. The profile uses a graph of Microsoft Excel in a bar chart to display the hourly angular range of azimuth and altitude on the four path periods. A latitude zone with a higher angular range for a year indicates a better position than other latitude zones. The dynamic position, which meaning it has a wide range of orientations and a balanced high elevation, which indicates the spreading position.

The fourth step (b) is to make a profile of the opportunity for the sloped surfaces to receive access. The profile created aims to illustrate the tilted surface arrangement facing the sun's position in the equatorial region. If the profile can show the spreading surfaces in four main orientations, this ensures opportunities for the inclined surfaces receiving access from many directions. Meanwhile, the rule for orientation is to follow the clockwise direction. The north orientation is 0° or 360°, followed by the east, south, and west at 90°, 180°, and 270°, respectively. The plus sign is for the angle in the northern hemisphere. The minus sign is for the angle in the southern hemisphere.

3. RESULTS AND DISCUSSION

The simulation results can be accepted and used for the next steps after comparing with the validation results, where the deviation between the two data is small (less than 0.2 degrees).

3.1. The Sun's Position Viewed from Latitude 35°N

Table 1 presents the recapitulation of AZI and ALT on the four sun path periods, viewed from

the observer at 35°N.

Table 1. The recapitulation of AZI and ALT viewed from latitude 35°N.

Latitude	Sun path Period	Angular Coordinate	Time Observation	Simulation (°)	ORI	Angular Range (°)	Validation (°)	Deviation (°)
35°N	Jun 21 (+23.45°)	Azimuth	09:00 a.m.	97.14	SE	171.56	97.15	-0.01
			03:00 p.m.	268.70	SW		268.72	-0.02
		Altitude	09:00 a.m.	53.12	-	24.66	53.15	-0.03
			Noon	77.78	-		77.78	0.00
	Dec 21 (-23.45°)	Azimuth	09:00 a.m.	141.40	SE	85.54	141.43	-0.03
			03:00 p.m.	226.94	SW		226.96	-0.02
		Altitude	09:00 a.m.	20.58	-	10.75	20.64	-0.06
			Noon	31.33	-		31.36	-0.03
	Mar 21 (0°)	Azimuth	09:00 a.m.	122.36	SE	120.93	122.45	-0.09
			03:00 p.m.	243.29	SW		243.18	0.11
		Altitude	09:00 a.m.	37.92	-	17.38	37.85	0.07
			Noon	55.30	-		55.20	0.10
	Sep 21 (0°)	Azimuth	09:00 a.m.	125.54	SE	120.53	125.42	0.12
			03:00 p.m.	246.07	SW		246.15	-0.08
		Altitude	09:00 a.m.	40.45	-	14.49	40.53	-0.08
			Noon	54.94	-		55.06	-0.12

3.1.1. June 21 and December 21 viewed from latitude 35°N

Figure 6 shows the horizontal and vertical sun-path diagrams on June 21 at latitude 23.45°N and December 21 at latitude 23.45°S, viewed from the observer in the north latitude. The lane on June 21 (green) with a more curved and tall line is the closest to the observer. The lane on December 21 (blue) with a slightly curved and short line is the farthest from the observer. The two paths show a significant difference in size. The azimuth range on June 21 (171.56°) is equivalent to twice the width on December 21 (85.54°). The altitude range on June 21 (24.66°) and the altitude at noon on June 21 (77.78°) are also twice the height on December 21: 10.75° and 31.33°, respectively.
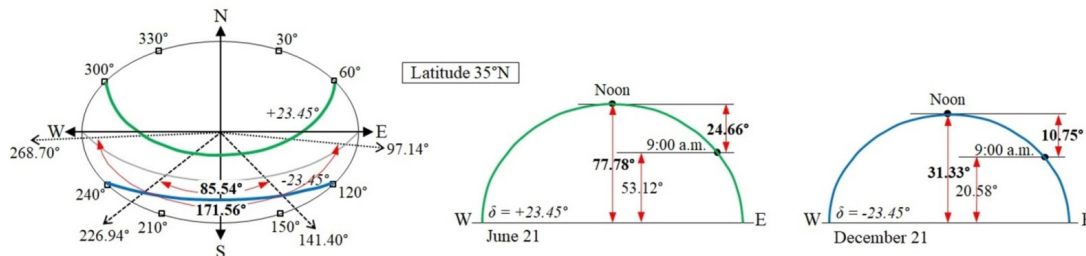
Figure 6. The horizontal and vertical sun path periods on June 21 and December 21, viewed from latitude 35°N.

The significant difference in the size of the two paths viewed from the north latitude is affected by the sun-earth relationship and the season periods. According to Figure 1, July 4 and January 3 are the farthest and the nearest sun-earth distance, respectively. June 21 has a bigger path size because it is closer to July 4 than December 21, which is close to January 3.

According to Figure 2, δ = +23.45° is the northern summer solstice on June 21. The area in the north latitude has a brighter surface due to facing directly to the northern summer solstice. The difference in the horizontal sun path of both conforms to Figure 3 in the case of Freiburg, Germany (Lat. 48°N), which has an asymmetrically curved sun path between June 21 and December 21. The path on the northern summer solstice on June 21 has a more curved line than the winter solstice. Meanwhile, the difference in the vertical track agrees with Figure 4a, which shows the higher semicircle track in the northern summer solstice on June 21 than the winter solstice on December 21.

Thus, the observer at 35°N receives the best access during the northern summer solstice.

3.1.2.   March 21 and September 21 viewed from latitude 35°N

Figure 7 displays the horizontal and vertical sun paths on March 21 and September 21, viewed from the observer in the north latitude. Both paths overlap at the equator (Lat. 0°) on one curved line (grey) pointing north but in opposite directions. On March 21, the path leads northward (June), while on September 21, it goes southward (December). Even though both paths coincide at the same position, there is a slightly different movement, particularly in vertical. The altitude range on March 21 is 17.38°, and the point of altitude at noon is 55.30°.

Meanwhile, on September 21, these values are slightly lower at 14.49° and 54.94°, respectively. Additionally, the azimuth range on March 21 (120.93°) is almost the same as on September 21 (120.53°).

The size difference between the two lanes viewed from the northern latitude is affected by the sun-earth relationship and the season periods. According to Figure 1, the path size on March 21 is slightly broader because it is towards the north (June 4 as aphelion), compared to September 21, which is towards the south (January 3 as perihelion). Figure 2 shows δ = 0° is the equinoxes at the equator on March 21 (vernal equinox) and September 21 (autumnal equinox). The area in the northern latitude exhibits a shadier surface due to facing obliquely to the equinoxes. The overlapping of horizontal sun paths corresponds to Figure 3 in the case of Freiburg, Germany (Lat. 48°N), which features a curved line that overlaps on March 21 and September 21.

The overlapping of vertical tracks aligns with Figure 4a, showing the equinoxes on March 21 and September 21 with the relatively same high of semicircle tracks but lower than the northern summer solstice on June 21. Hence, the observer at 35°N receives less access during the equinoxes.
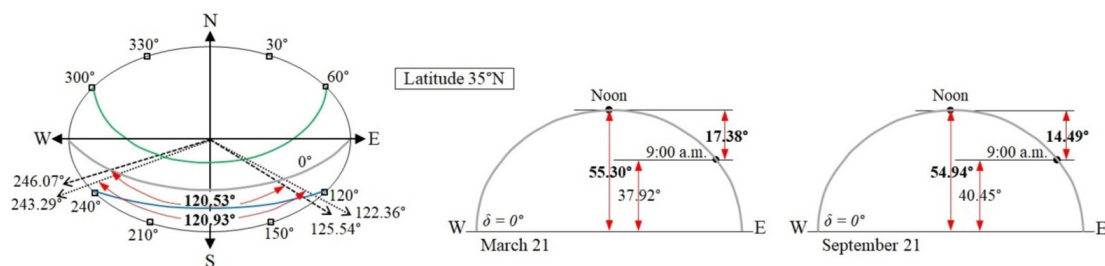
Figure 7. The horizontal and vertical sun path periods on March 21 and September 21, viewed from latitude 35°N.

3.2. The Sun's Position Viewed from Latitude 0°

Table 2 presents the recapitulation of AZI and ALT on the four sun path periods, viewed from the observer at latitude 0°.

Table 2. The recapitulation of AZI and ALT viewed from latitude 0°.

Latitude	Sun path Period	Angular Coordinate	Time Observation	Simulation (°)	ORI	Angular Range (°)	Validation (°)	Deviation (°)
0°	Jun 21 (+23.45°)	Azimuth	09:00 a.m.	56.26	SE	116.58	56.25	0.01
			03:00 p.m.	299.68	SW		299.67	0.01
		Altitude	09:00 a.m.	44.27	-	21.88	44.31	-0.04
			Noon	66.15	-		66.16	-0.01
	Dec 21 (-23.45°)	Azimuth	09:00 a.m.	124.26	SE	116.39	124.28	-0.02
			03:00 p.m.	240.65	SW		240.66	-0.01
		Altitude	09:00 a.m.	45.04	-	20.93	45.09	-0.05
			Noon	65.97	-		65.97	0.00
	Mar 21 (0°)	Azimuth	09:00 a.m.	89.43	SE	178.79	89.60	-0.17
			03:00 p.m.	270.64	SW		270.50	0.14
		Altitude	09:00 a.m.	48.21	-	38.54	48.21	0.00
			Noon	86.75	-		86.78	-0.03
	Sep 21 (0°)	Azimuth	09:00 a.m.	89.10	SE	178.50	88.92	0.18
			03:00 p.m.	270.60	SW		270.73	-0.13
		Altitude	09:00 a.m.	51.73	-	31.51	51.72	0.01
			Noon	83.24	-		83.25	-0.01

3.2.1. June 21 and December 21 viewed from latitude 0°

Figure 8 shows the horizontal and vertical sun-path diagrams on June 21 and December 21, viewed from the observer at the equator (Lat. 0°). The paths on June 21 (green) in the north and December 21 (blue) have the opposite curvature of lines and directions. The altitude range on June 21 (21.88°) and the altitude at noon on June 21 (66.15°) are slightly higher than December 21: 20.93° and 65.97°, respectively. The azimuth range on June 21 (116.58°) is almost the same width on December 21 (116.39°).
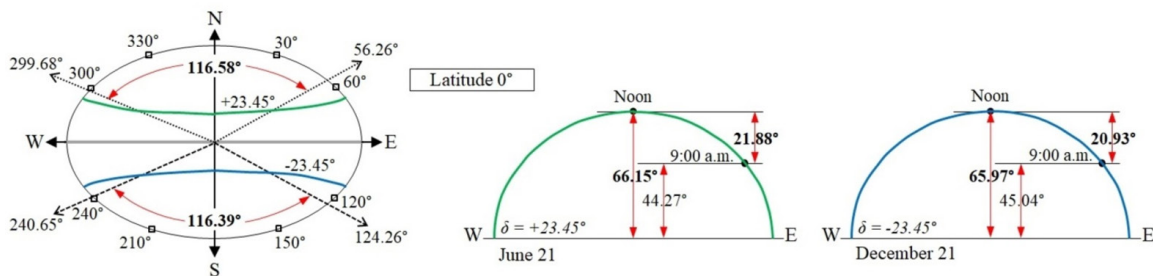
Figure 8. The horizontal and vertical sun path periods on June 21 and December 21, viewed from latitude 0°.

The slight difference in the size of the two paths viewed from the equator is affected by the sun-earth relationship and the season periods. According to Figure 1, July 4 and January 3 are the farthest and the nearest sun-earth distance, respectively. June 21 has a slightly higher path size because it is closer to July 4 than December 21, which is close to January 3. According to Figure 2, δ = +23.45° is the northern summer solstice on June 21, and δ = -23.45° is the southern summer

solstice on December 21. The area at the equator has a sunnier surface due to facing directly to the sun in two directions (north and south) in balance. The opposite horizontal sun path of both conforms to Figure 3 in the case of Singapore (Lat. 1°N), which has a symmetrically curved sun path between June 21 and December 21. Meanwhile, the opposite vertical track agrees with Figure 4b, which shows similar heights between the summer solstices in the north and south. Thus, the observer at the equator receives good access from the two summer solstices.

3.2.2. March 21 and September 21 viewed from latitude 0°

Figure 9 displays the horizontal and vertical sun paths on March 21 and September 21, viewed from the observer at the equator (Lat. 0°).

Both paths overlap in the same position and unify with the observer in a straight line (grey) but with different directions.

On March 21, the path leads northward, while on September 21, the path goes southward. Even though both paths coincide at the same position, there is a slight difference in movement, particularly in vertical.

The altitude range on March 21 is 38.54°, and the point of altitude at noon is 86.75°. Meanwhile, on September 21, these values are slightly lower at 31.51° and 83.24°, respectively. The azimuth range on March 21 (178.79°) is somewhat higher than on September 21 (178.50°).
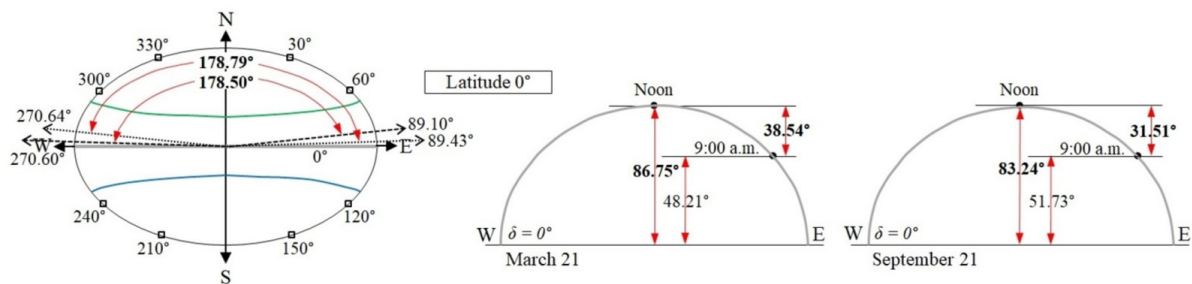
Figure 9. The horizontal and vertical sun path periods on March 21 and September 21, viewed from latitude 0°.

The size difference between the two lanes viewed from the equator is affected by the sun-earth relationship and the season periods.

According to Figure 1, the path size on March 21 is slightly broader because it is towards the north (June 4 as aphelion), compared to September 21, which is towards the south (January 3 as perihelion). Figure 2 shows that $\delta = 0°$ is the equinoxes at the equator on March 21 (vernal equinox) and September 21 (autumnal equinox). The area at the equator exhibits the brightest surface as it directly faces perpendicular to the equinoxes. The overlapping of horizontal sun paths corresponds to Figure 3 in the case of Singapore (Latitude 1°N), which features a single straight line that overlaps on March 21 and September 21.

The overlapping of vertical tracks aligns with Figure 4b, showing the equinoxes on March 21 and September 21 are the highest semicircle tracks. The equinoxes pass at the equator flanked by the summer solstice in the north and south, which have a lower semicircular track.

Hence, the observer at the equator receives the best access during the equinoxes.

3.3. The Sun's Position Viewed from Latitude 35°S

Table 3 presents the recapitulation of AZI and ALT on the four sun path periods, viewed from the observer at latitude 35°S.

Table 3. The recapitulation of AZI and ALT viewed from latitude 35°S.

Latitude	Sun path Period	Angular Coordinate	Time Observation	Simulation (°)	ORI	Angular Range (°)	Validation (°)	Deviation (°)
35°S	Jun 21 (+23.45°)	Azimuth	09:00 a.m.	39.35	SE	85.63	39.33	0.02
			03:00 p.m.	313.72	SW		313.71	0.01
		Altitude	09:00 a.m.	20.10	-	11.31	20.16	-0.06
			Noon	31.41	-		31.43	-0.02
	Dec 21 (-23.45°)	Azimuth	09:00 a.m.	82.19	SE	171.43	82.17	0.02
			03:00 p.m.	270.76	SW		270.74	0.02
		Altitude	09:00 a.m.	53.88	-	23.62	53.92	-0.04
			Noon	77.50	-		77.49	0.01
	Mar 21 (0°)	Azimuth	09:00 a.m.	56.98	SE	119.44	57.09	-0.11
			03:00 p.m.	297.54	SW		297.45	0.09
		Altitude	09:00 a.m.	37.37	-	17.07	37.47	-0.10
			Noon	54.44	-		54.57	-0.13
	Sep 21 (0°)	Azimuth	09:00 a.m.	53.50	SE	118.78	53.43	0.07
			03:00 p.m.	294.72	SW		294.84	-0.12
		Altitude	09:00 a.m.	39.61	-	14.32	39.53	0.08
			Noon	53.93	-		53.84	0.09

3.3.1. December 21 and June 21 viewed from latitude 35°S

Figure 10 shows the horizontal and vertical sun-path diagrams on December 21 at latitude 23.45°S and June 21 at latitude 23.45°N, viewed from the observer in the south latitude. The lane on December 21 (blue) with a more curved and tall line is the closest to the observer. The lane on June 21 (green) with a slightly curved and short line is the farthest from the observer. The two paths show a significant difference in size. The azimuth range on December 21 (171.43°) is twice the width on June 21 (85.63°). The altitude range on December 21 (23.62°) and the altitude at noon on December 21 (77.50°) are also twice the height on June 21: 11.31° and 31.41°, respectively.
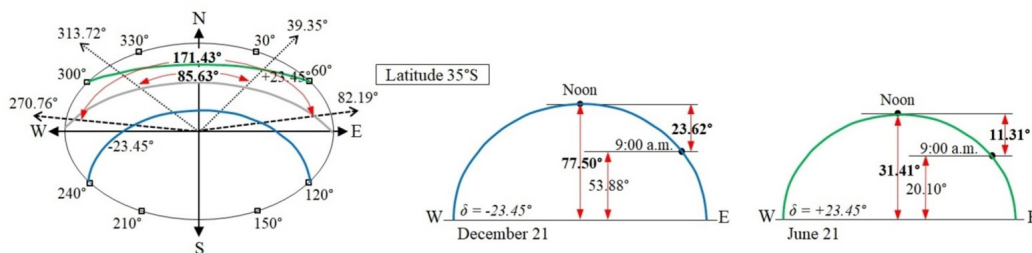
Figure 10. The horizontal and vertical sun path periods on December 21 and June 21, viewed from latitude 35°S.

The significant difference in the size of the two paths viewed from the south latitude is affected by the sun-earth relationship and the season periods. According to Figure 1, January 3 and July 4 are the nearest and the farthest sun-earth distance, respectively. December 21 is more influenced by the change of seasons because the sun-earth distance in the south is shorter than in the north. According to Figure 2, δ = -23.45° is the summer solstice on December 21. The area in the south latitude has a brighter surface due to facing directly to the southern summer solstice at 23.45°S.

The difference in the horizontal sun path of both conforms to Figure 3 in the case of Florianopolis, Brazil (Lat. 27°S), which has an asymmetrically curved sun path between December 21 and June 21. The path on the southern summer solstice on December 21 has a more curved line than the winter solstice. Meanwhile, the difference in the vertical track agrees with Figure 4a, which shows the higher semicircle track in the southern summer solstice on December 21 than the winter solstice on June 21. Thus, the observer at 35°S receives the best access during the summer solstice in the south.

3.3.2. September 21 and March 21 viewed from latitude 35°S

Figure 11 displays the horizontal and vertical sun paths on September 21 and March 21, viewed from the observer in the south latitude. Both paths overlap at the equator on one curved line (grey) pointing south but in opposite directions. On September 21 is the cycle that leads southward, while on March 21 is the cycle that goes northward. Even though both paths coincide at the same position, there is a slight difference in vertical movement. The altitude range on September 21 is 14.32°, and the point of altitude at noon is 53.93°. Meanwhile, on March 21, these values are slightly higher at 17.07° and 54.44°, respectively. The azimuth range on September 21 (118.78°) is almost the same as on March 21 (119.44°).
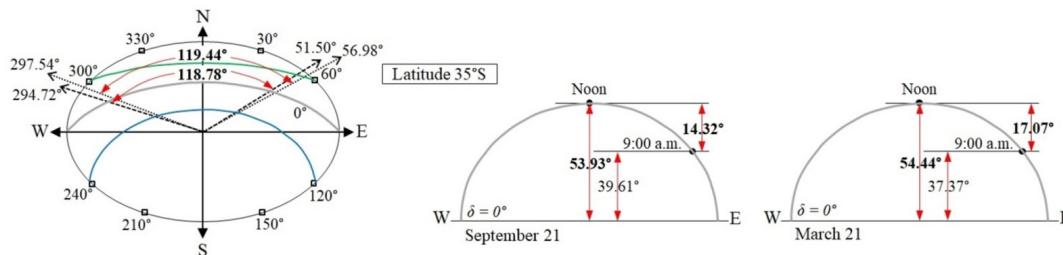
Figure 11. The horizontal and vertical sun path periods on September 21 and March 21, viewed from latitude 35°S.

The size difference between the two paths viewed from the south latitude is affected by the sun-earth relationship and the season periods. According to Figure 1, the path size on September 21 is slightly narrower because it is towards the south (January 3 as perihelion), compared to March 21, which is towards the north (July 4 as aphelion). Figure 2 shows δ = 0° is the equinoxes at the equator on September 21 (vernal equinox) and March 21 (autumnal equinox). The area in the south latitude exhibits a shadier surface because it faces obliquely to the equinoxes. The overlapping of horizontal sun paths corresponds to Figure 3 in the case of Florianopolis, Brazil (Lat. 27°S), which features a curved line that overlaps on September 21 and March 21. The overlapping of vertical tracks aligns with Figure 4a, showing the equinoxes on September 21 and March 21 with the relatively same high of semicircle tracks but lower than the southern summer solstice on December 21. Hence, the observer at latitude 35°S receives less access during the equinoxes.

The difference in the angular range of AZI and ALT is the characteristic of the sun's position in each latitude zone. The summaries of the discussions are as follows:
• The range of AZI or orientation from 9:00 a.m. to 3:00 p.m. above 100 degrees:
    For latitude 0° includes four sun path periods: June 21 (116.58°), December 21 (116.39°), March 21 (178.79°), and September 21 (178.50°). For latitude 35°N includes three sun path periods: June 21 (171.56°), March 21 (120.93°), and September 21 (120.53°), while for latitude 35°S: December 21 (171.43°), March 21 (119.44°), and September 21 (118.78°). The total range for latitude 0° (590.26°) is higher than latitude 35°N (498.56°) and latitude 35°S (495.28°).
• The range of ALT or elevation from 9:00 a.m. to noon above 20 degrees:
    For latitude 0° includes four sun path periods: June 21 (21.88°), December 21 (20.93°),

March 21 (38.54°), and September 21 (31.51°). For latitude 35°N includes one sun path period: June 21 (24.66°), while for latitude 35°S: December 21 (23.62°). The total range for latitude 0° (112.86°) is higher than latitude 35°N (67.28°) and latitude 35°S (66.32°).

• The point of ALT or elevation at noon above 60 degrees:

For latitude 0° includes four sun path periods: June 21 (66.15°) in the north, December 21 (65.97°) in the south, and March 21 (86.75°) and September 21 (83.24°).

For latitude 35°N includes one sun path period: June 21 (77.78°), while for latitude 35°S: December 21 (77.50°).

Latitude 0°, which has a range of AZI of more than 100 degrees on the four sun path periods, describes the broad orientation. Latitude 0°, which has a range of ALT of more than 20 degrees on the four sun path periods, indicates the balance elevation. Latitude 0°, which has the point of ALT at noon relatively perpendicular on two sun path periods, demonstrates the highest elevation in a long period. The high average angular range horizontally and vertically allows the tilted surfaces to receive access from many directions due to the spreading sun's position in the equatorial region.

All phenomena observed follow the latitude function and the time function. The elliptical orbit of the Earth causes a difference in the sun-earth distance. The declination angle shift in the change of seasons causes different exposure on the surface side of the Earth. The sun's position viewed from the northern hemisphere is the opposite as viewed from the southern hemisphere. However, the angular range in the north latitude is slightly broader than in the south latitude. Meanwhile, the phenomenon of the sun's position viewed from the equator shows privilege because its region is crossed by the sun twice a year in balance. Hence, the sun's position in this region has a broader angular range horizontally and a balanced angular range vertically than the other latitude zones. Figure 12 displays the performance of the sun's position at three latitude zones. The graph discloses the characteristics of the sun's position at each latitude zone. The angular observed include azimuth angle range (blue), altitude angle range (red), and altitude angle at noon (green). Latitude 0° has a better performance of the sun's position than other latitude zones.
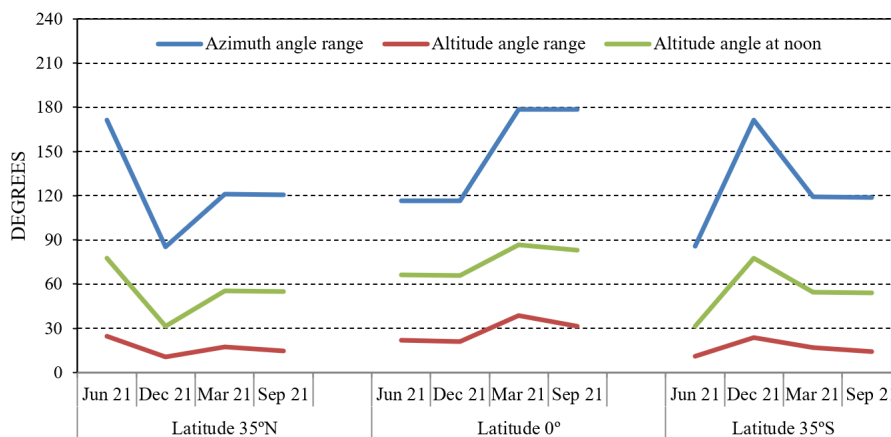
Figure 12. The performance of the sun's position at three latitudes: 35°N, 0°, and 35°S.

Latitude 0° has a high average angular range on four sun path periods: March 21, September 21, June 21, and December 21. The equinoxes are the best angular range, on March 21 with an azimuth range of 178.79°, an altitude range of 38.54°, and a noon position of 86.75°. The equinox on September 21 also exhibits high angular ranges. Meanwhile, latitude 35° has a high average angular range only during one sun path period: June 21 for latitude 35°N and December 21 for latitude 35°S. For latitude 35°N, the azimuth range is 171.56°, the altitude range is 24.66°, and the noon position is 77.78°. For latitude 35°S, the azimuth range is 171.43°, the altitude range is

23.62°, and the noon position is 77.50°. Thus, latitude 0° shows a balanced position throughout the year, while latitudes 35°N and 35°S show a focus on one sun path period in summer.

The implications of the sun's position in the subtropical regions show the suitability. In the north, Choi [36] in Korea studied kinetic solar panels on south-facing building facades to maximize energy generation. Similarly, Qadourah et al. [37] showed the roof and façade facing south as the highest radiation reception for solar panels in Jordan. Meanwhile, Balter et al. [38] in Argentina investigated north-facing facades and roofs to improve building energy performance. Yang et al. [39] observed photovoltaic/thermal collectors on north-facing double-skin facades to increase energy efficiency in Australia. However, the equatorial region has not utilized comprehensively the character of the sun's position that spreads. Here, the influence of the subtropical region approach is still dominant in optimum studies.
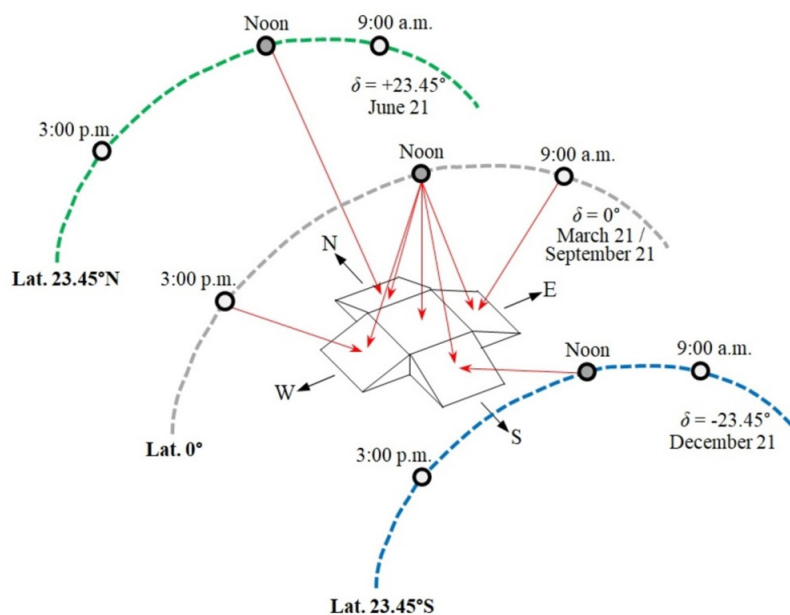
Figure 13. The profile of the opportunity for the tilted surface to receive access.

The profile in Figure 12 has proven that the spreading sun's position in the equatorial region. Figure 13 illustrates the profile of the opportunity of the inclined surfaces to receive access. The tilted surfaces in the equinoxes on March 21 and September 21 show the best opportunity for exposure from many orientation directions because it is the highest position and the longest period. The tilted surfaces in the summer solstices on June 21 and December 21 show the opportunity for exposure from one orientation because it is the farthest sun's position in the north and south, respectively.

The equinoxes are the center of access for location at the equator because the sun passes twice a year with opposite cycles, so it has a long period covering spring and autumn. The highest sun's position in the equinoxes allows the low-inclined surfaces in opposite orientations facing four cardinal directions to receive access concurrently. This is the optimum potential in the equatorial region, which can be obtained with many combinations of orientation and tilt angle.

4. CONCLUSIONS

The findings from the study are as follows:

• The sun-earth relationship due to the elliptical orbit of the Earth and the season periods due to the declination angle shift are parameters that cause differences in angular ranges as a character

of the sun's position for each latitude zone.

• The equatorial region has a broader orientation range and relatively balanced altitude during the year than other regions, as measured in the following three angular range conditions.

- o The range of orientation from 9 a.m. to 3 p.m. with angles above 100 degrees on latitude 0° includes four sun path periods: March 21 (178.79°), September 21 (178.50°), June 21 (116.58°), December 21 (116.39°). While, latitude 35°N includes three periods: June 21 (171.56°), March 21 (120.93°), and September 21 (120.53°). Similarly, latitude 35°S experiences three periods: December 21 (171.43°), March 21 (119.44°), and September 21 (118.78°).

- o The range of elevation from 9 a.m. to noon with angles above 20 degrees on latitude 0° includes three sun path periods: March 21 (38.54°), September 21 (31.51°), June 21 (21.88°), December 21 (20.93°). Latitude 35°N experiences one period: June 21 (24.66°), and also latitude 35°S on one period: December 21 (23.62°).

- o The elevation at noon with angles above 60 degrees on latitude 0° includes four sun path periods: March 21 (86.75°), September 21 (83.24°), June 21 (66.15°), and December 21 (65.97°). Meanwhile, latitude 35°N experiences one period: June 21 (77.78°), and also latitude 35°S on one period: December 21 (77.50°).

It proves the equatorial region has geographical advantages from the sun's position that spreads, so there is an opportunity for the two low-sloped surfaces in opposite orientations to receive access at the same time. These results confirm its suitability with a group of solar energy studies in the equatorial region that stated the optimum orientation facing non-perpendicular, as shown by [13], [14], [15], [16], [17], [18], [19].

• This study contributes in-depth knowledge of the dynamic position in the equatorial region, which opens an opportunity to receive solar access that is not monotonous with one orientation but with many. In a sustainable context, urban settlements in the equatorial region have the potential to utilize the varying roof configurations with integrated photovoltaics to provide clean energy needs at the community level.

REFERENCES

[1] IPCC, "9-Buildings," in Climate Change 2022: Mitigation of climate change. Cambridge: Cambridge University Press, 2022, pp. 953–1048, doi: 10.1017/9781009157926.011.

[2] N. P. Hariram, K. B. Mekha, V. Suganthan, and K. Sudhakar, "Sustainalism: An integrated socio-economic-environmental model to address sustainable development and sustainability," Sustain., vol. 15, no. 13, p. 10682, 2023, doi: 10.3390/su151310682.

[3] M. Soroush and Y. Hajimolana, "Sunlight harvesting," Comput. Chem. Eng., vol. 170, p. 108103, 2023, doi: 10.1016/j.compchemeng.2022.108103.

[4] T. Guney, "Solar energy, governance and CO2 emissions," Renew. Energy, vol. 184, pp. 791–798, 2022, doi: 10.1016/j.renene.2021.11.124.

[5] J. A. Duffie, W. A. Beckman, and N. Blair, Solar engineering of thermal processes, photovoltaics and wind. New Jersey: John Wiley & Sons, 2020, doi: 10.1002/9781119540328.

[6] G. Y. Kim, D. S. Han, and Z. Lee, "Solar panel tilt angle optimization using machine learning model: A case study of Daegu city, South Korea," Energies, vol. 13, p. 529, 2020, doi: 10.3390/

en13030529.

[7] S. Sevik, A. Kocer, H. Ince, and F. E. Tombus, "Determination of optimum tilt angle of the solar collector and evaluation of the position of the existing buildings in terms of solar potential," Archit. Eng. Des. Manag., vol. 18, no. 6, pp. 812–828, 2022, doi: 10.1080/17452007.2021.1926899.

[8] M. M. Cabral, S. A. Lemes, M. E. de Oliveira, P. H. A. Silva e Silva, and G. P. Viajante, "Software for calculating the optimum tilt angle of PV modules in different latitudes of the southern hemisphere and solar plant sizing," Renew Energy Power Qual J., vol. 19, pp. 304–309, 2021, doi: 10.24084/repqj19.282.

[9] M. E. Matius et al., "On the optimal tilt angle and orientation of an on-site solar photovoltaic energy generation system for sabah's rural electrification," Sustain., vol. 13, no. 10, p. 5730, 2021, doi: 10.3390/su13105730.

[10] H. O. Njoku, U. G. Azubuike, E. C. Okoroigwe, and O. V. Ekechukwu, "Tilt angles for optimizing energy reception by fixed and periodically adjusted solar-irradiated surfaces in Nigeria," Int. J. Energy Water Resour., vol. 4, no. 4, pp. 437–452, 2020, doi: 10.1007/s42108-020-00072-7.

[11] A. Afandi, M. D. Birowosuto, and K. C. Sembiring, "Energy-yield assessment based on the orientations and the inclinations of the solar photovoltaic rooftop mounted in Jakarta, Indonesia," Int. J. Adv. Sci. Eng. Inf. Technol., vol. 12, no. 2, pp. 470–476, 2022, doi: 10.18517/ijaseit.12.2.14812.

[12] I. B. K. Sugirianta, I. G. A. M. Sunaya, and I. G. N. A. D Saputra, "Optimization of tilt angle on-grid 300Wp PV plant model at Bukit Jimbaran Bali," J. Phys. Conf. Ser., vol. 1450, p. 012135, 2020, doi: 10.1088/1742-6596/1450/1/012135.

[13] X. Serrano-Guerrero, D. Alvarez-Lozano, and S. F. L. Romero, "Influence of local climate on the tilt and orientation angles in fixed flat surfaces to maximize the capture of solar irradiation: A case study in Cuenca-Ecuador," in IEEE International Autumn Meeting on Power, Electronics and Computing, Ixtapa, Mexico, 13–15 November 2019, pp. 91–96, doi: 10.1109/ROPEC48299.2019.9057102.

[14] Y. S. Khoo et al., "Optimal orientation and tilt angle for maximizing in-plane solar irradiation for PV applications in Singapore," IEEE J. Photovoltaics, vol. 4, no. 2, pp. 647–653, 2014, doi: 10.1109/JPHOTOV.2013.2292743.

[15] S. Bari, "Optimum orientation of domestic solar water heaters for the low latitude countries," Energy Convers. Manag., vol. 42, no. 10, pp. 1205–1214, 2001, doi: 10.1016/S0196-8904(00)00135-7.

[16] K. Y. Lau, C. W. Tan, and A. H. M. Yatim, "Effects of ambient temperatures, tilt angles, and orientations on hybrid photovoltaic/diesel systems under equatorial climates," Renew. Sustain. Energy Rev., vol. 81, no. 2, pp. 2625–2636, 2018, doi: 10.1016/j.rser.2017.06.068.

[17] J. Cronemberger, E. Caamano-Martin, and S. V. Sanchez, "Assessing the solar irradiation potential for solar photovoltaic applications in buildings at low latitudes - Making the case for Brazil," Energy Build., vol. 55, pp. 264–272, 2012, doi: 10.1016/j.enbuild.2012.08.044.

[18] K. E. N'Tsoukpoe, "Effect of orientation and tilt angles of solar collectors on their performance: Analysis of the relevance of general recommendations in the West and Central African context," Sci. African, vol. 15, p. e01069, 2022, doi: 10.1016/j.sciaf.2021.e01069.

[19] N. Mukisa and R. Zamora, "Optimal tilt angle for solar photovoltaic modules on pitched rooftops: A case of low latitude equatorial region," Sustain. Energy Technol. Assessments, vol. 50, p. 101821, 2022, doi: 10.1016/j.seta.2021.101821.

[20] UN. Population Division, World population prospects 2019: Highlights (ST/ESA/ SER.A/423). New York: United Nations, 2019. Available: https://digitallibrary.un.org/record/3813698?ln=en&v=pdf.

[21]   UN. Department of Economic and Social Affairs, Global sustainable development report 2023: times of crisis, times of change science for accelerating transformations to sustainable development. New York: United Nations, 2023. Available: https://digitallibrary.un.org/ record/4018896?ln=en&v=pdf.

[22]   G. Notton, "Solar radiation for energy applications," in Encyclopedia of Sustainable Technologies. Amsterdam: Elsevier, 2017, pp. 339–356, doi: 10.1016/B978-0-12-409548-9.10130-7.

[23]   W. T. Grondzik and A. G. Kwok, Mechanical and electrical equipment for buildings. New York: John Wiley & Sons, 2014.

[24]   D. Y. Goswami, Principles of solar engineering. Boca Raton: CRC Press, 2022, doi: 10.1201/9781003244387.

[25]   A. M. Nobre, "Short-term solar irradiance forecasting and photovoltaic systems performance in a tropical climate in Singapore", Dr. Eng. dissertation, Universidade Federal de Santa Catarina, Florianopolis, Brazil, 2015, doi: 10.13140/RG.2.1.2195.3683.

[26]   S. V. Szokolay, Introduction to architectural science: The basis of sustainable design. New York: Routledge, 2014, doi: 10.4324/9781315852409.

[27]   mydarksky.org, Solstices and equinoxes. [Online]. Available: https://mydarksky. org/2009/12/22/solstices-and-equinoxes/. [Accessed: Aug. 26, 2022].

[28]   J. Henry, "Tropical and equatorial climates," in Encyclopedia of world climatology. Dordrecht: Springer, 2005, pp. 742–750, doi: 10.1007/1-4020-3266-8_212.

[29]   SunEarthTools.com, SunEarthTools.com-Tools for consumers and designers of solar. [Online]. Available: https://www.sunearthtools.com. [Accessed: Apr. 22, 2022].

[30]   J. J. Michalsky, "The Astronomical Almanac's algorithm for approximate solar position (1950–2050)," Sol. Energy, vol. 40, no. 3, pp. 227–235, 1988, doi: 10.1016/0038-092X(88)90045-X.

[31]   GML-NOAA, Solar calculation details. [Online]. Available: https://gml.noaa.gov/grad/ solcalc/calcdetails.html. [Accessed: Dec. 27, 2023].

[32] J. Meeus, Astronomical Algorithms, Richmond, VA: Willmann-Bell, Inc., 1998.

[33]   F. R. Shapiro, "The position of the sun based on a simplified model," Renew. Energy, vol. 184, pp. 176–181, 2022, doi: 10.1016/j.renene.2021.11.084.

[34]   A. Jenkins, "The Sun's position in the sky," Eur. J. Phys., vol. 34, no. 3, p. 633, 2013, doi: 10.1088/0143-0807/34/3/633.

[35]   T. P. Chang, "The Sun's apparent position and the optimal tilt angle of a solar collector in the northern hemisphere," Sol. Energy, vol. 83, no. 8, pp. 1274–1284, 2009, doi: 10.1016/j. solener.2009.02.009.

[36]   H. S. Choi, "Architectural experiment design of solar energy harvesting: A kinetic façade system for educational facilities," Appl. Sci., vol. 12, no. 12, p. 5853, 2022, doi: 10.3390/ app12125853.

[37]   J. A. Qadourah, A. Alfalahat, and S. Alrwashdeh, "Assessment of solar photovoltaics potential installation into multi-family building's envelope in Amman, Jordan," Cogent Eng., vol. 9, no. 1, p. 2082059, 2022, doi: 10.1080/23311916.2022.2082059.

[38]   J. Balter, G. Barea, and C. Ganem, "Improvements in the energy performance of buildings in summer, through the integration of ventilated envelopes on north-facing facades and roofs. The case of Mendoza, Argentina," Habitat Sustentable, vol. 10, no. 2, pp. 94–105, 2020, doi: 10.22320 /07190700.2020.10.02.07.

[39]   S. Yang, A. Cannavale, A. D. Carlo, D. K. Prasad, A. Sproul, and F. Fiorito, "Performance assessment of BIPV/T double-skin façade for various climate zones in Australia: Effects on energy consumption," Sol. Energy, vol. 199, pp. 377–399, 2020, doi: 10.1016/j.solener.2020.02.044.